AirCargoChallenge 2022

Technical Report

Team #07

Team Beoavia

BEO AVIA

a member of EUROAVIA

CONTENTS

1   INTRODUCTION

Project "Phoenix" is a project organized by team "Beoavia" centered in the University of Belgrade for the purpose of competing in Air Cargo Challenge in Munich. Majority of students are from the Faculty of Mechanical Engineering with significant portion of members from other faculties, including The Faculty of Technology and Metallurgy, Organized science, The Faculty of Electrical Engineering etc. Main goal is for students to gain knowledge and experience through engaging in practical problems solving. Team itself consists of five subdivisions in respect to problem solving tasks of project. Subdivisions are: Aerodynamics, Propulsion, Electronics, Marketing and Structure & Manufacturing.

Every group had a meeting once per week where it was discussing about previous work and what tasks are upcoming. There were two meetings per month where the whole team was gathering and had briefing about the work of the other sections. Every section is organized by its coordinator, who is obligated to give out tasks for their members. Those tasks are handed by project coordinator who is entitled to keep track of deadlines and also helps the group to work as a whole. The idea of this type of organization is to enable the members of every section to work in their area of interest in a such way that every member is fully motivated to contribute to the project.

The team coordinator has many tasks. First of all, he should accomplish that every section gets the required items on time such as: tools, materials, software etc. Checking deadlines that defined coordinator of a project is duty of team coordinator. Also, he should fulfill the needs of every team member and motivate them, so he often organizes team building. Team coordinator has secretary who assists him in ordering items needed for a project.

Following the regulations of the competition, it is necessary to design an UAV aircraft which uses the AXI 2826/10 Gold Line V2 electric motor, a propeller and a three-cell battery. Furthermore, aircraft must fit in boxing unit with dimensions 1100x400x250 mm and also must fit in a "pre-flight" box with dimensions 1500x1500x500 mm. The mission of the ACC 2022 competition consists of following tasks: take-off, the main part of the mission and landing by caring blood transfusion bags in their cargo bay.

It is imperative that take-off is executed on the 60 m runway length and then prepare for the main part of the mission. The main goal is to flight larger distance with heavier payload as possible in two minutes. Time starts counting when an aircraft reaches the maximum altitude 60 seconds after take-off. Bonus points get if an aircraft takes-off in distance less than 40 meters, if payload is loading and unloading in satisfy time and if real payload mass is equal as predicted.

2 PROJECT MANAGEMENT

2.1 COST ESTIMATION

In this section, the estimated cost for the manufacturing of one our aircraft will be presented (table 2.1). The estimate elaborates the costs for material, manufacturing, structural, and propulsion components. Also, it elaborates the cost of every component that will be used on this aircraft. Please take notice that all prices are in euros. Three different prices are shown: base price, customs tax (10%), and price tax (20%). The price relevant for us is without tax because the University of Belgrade is tax-exempt for student NPO.

Table 2.1 – *Cost estimation (all prices in euro value)*

Component name	Oty	Unit price	Price	Component name	Oty	Unit price	Price
Material for production	1	875.00	875.00	Batery	2	8.77	17.54
Telemetry	1	161.66	161.66	Material for mold making	1	490.00	490.00
Propeller for horizontal flight	1	9.63	9.63	Wires and others	1	25.00	25.00
Motor for horizontal flight	1	98.00	98.00				
Electronic stablity control	1	25.00	25.00			Base price	1902.22
Landing gear	1	14.19	14.19			Customs(10%)	121.74
Tailwheel	1	6.00	6.00			Tax(20%)	2404.40
Servo motor	5	36.04	180.20			Total	2023.96

2.2 PROJECT SCHEDULE

The team uses a milestone chart, shown below (fig. 2.1), to keep track of the progress of the project. Milestone chart ensures that deadlines are respected and that aircraft is ready on time for the competition. The team has already finished the prototype aircraft on time. Currently, we are in the manufacturing of competition aircraft stage. In May, we are planning to start flight testing.
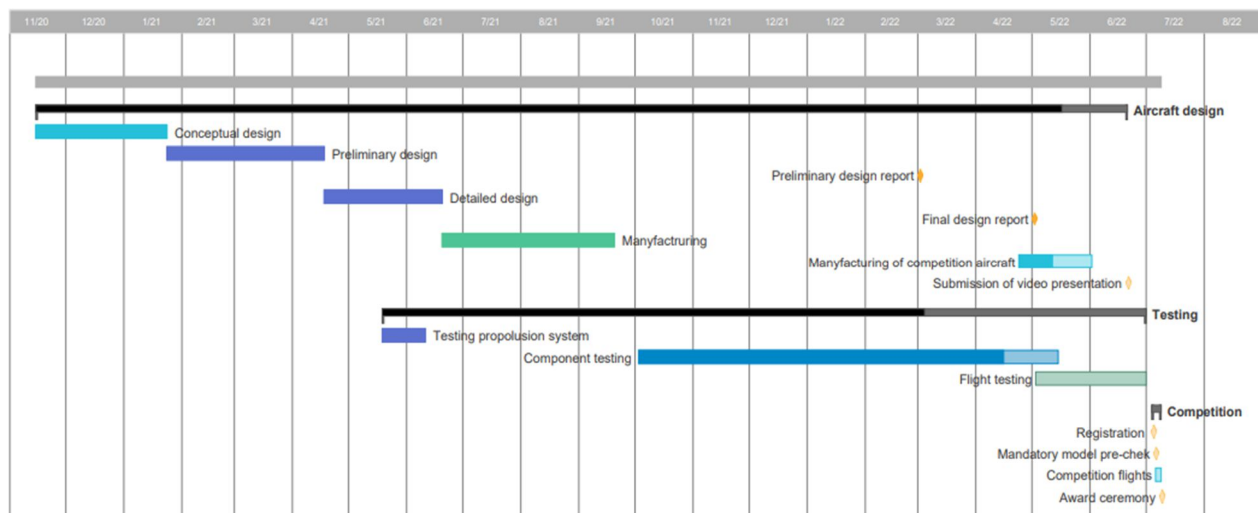

Figure 2.1-*Project milestone*

3 AERODYNAMICS DESIGN

The aerodynamics design of the aircraft consists of several phases which will be mentioned later in the report. This, it is essential to define the airfoils of the lift surfaces and then to execute the required dimensioning based on those aerodynamic characteristics.

3.1 "PRE-FLIGHT" BOX AND TRANSPORT BOX

Based on the previous study of the rules and physical limitations of the "Air Cargo Challenge 2022", competition, the most important condition in terms of sizing the aircraft are the physical limitations which, for this competition, are reflected in the "pre-flight box" and transport box. The focus is on the "pre-flight" box and based on its dimensions (1500×1500×500 mm), unambiguously defined global preliminary dimensions of the aircraft. Type of aircraft that has been considered and adopted is the classic configuration and trapezoidal wing shape. In this way, we managed to meet all the requirements of the competition (pre-flight and transport box) as well as meet the required aerodynamic characteristics.
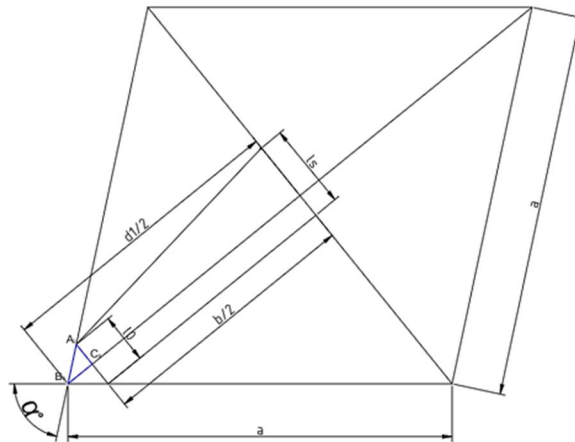

Figure 3.1 – Considering the pre-flight box problem

3.2 AIRFOILS

Overall, the airfoil effect: 1) Cruising speed
2) Runway length (which in our case cannot be longer than 60m);
3) Stalling speed;
4) Flight quality;
5) Overall flight efficiency.

Instead of using airfoils with a high lift coefficient, it was decided that we use an airfoil with a slightly less lift coefficient, but also to produce less drag in domain of the expected angles of attack.

With this being said, a list of priorities was created, and it consisted of:

• An airfoil that provides the wing with maximum lift coefficient $C_{L_{max}} = 1.5 \div 2.2$
• An airfoil that provides the wing with optimal lift coefficient $C_{L_{opt}} = 0.7 \div 1.0$
• Allows maximum lift to drag ratio in larger domain of angle of attacks (AoA)
• Maximum lift to drag ratio is on higher lift coefficient
• Not too thin trailing edge for easier and more precise production

Using various databases of airfoils, that are used to function properly in the domain of Reynolds numbers between 60 000 and 300 000, more than 30 airfoils were analyzed. Upon further analysis, three airfoils were singled out that mostly meet our requirements. The first airfoil that was taken into consideration was the S 1223, which has an exceptional maximum lift coefficient, but on the other hand, it creates high drag. The moment coefficient around its aerodynamic center is around $C_{m\ ac} \approx -0.29$. The airfoil creates a considerable lift coefficient even at low angles of attack, but a wing with this airfoil would create high induced drag. The second airfoil which was taken into consideration was the S 1210, which would give the wing $C_{L_{max}} = 1.6$ which meets our requirements, but at the same time, it enables the aircraft to have a higher lift to drag ratio, because of the lower drag created by the shape of the airfoil itself. E423 was also examined as a potential candidate, however, it has the lowest lift coefficient of all of the previously mentioned.
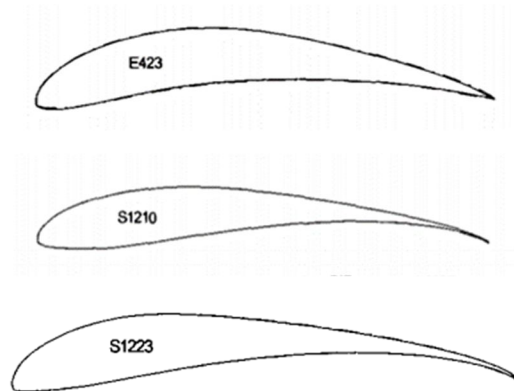

Figure 3.2 – *Chosen airfoils*

Looking through the airfoil database, which was created using empirical data, airfoil that best meets our requirements was the S1210. The only requirement that this airfoil did not meet was a thin trailing edge, but due to other advantages that this airfoil has, we decided to neglect that fact.
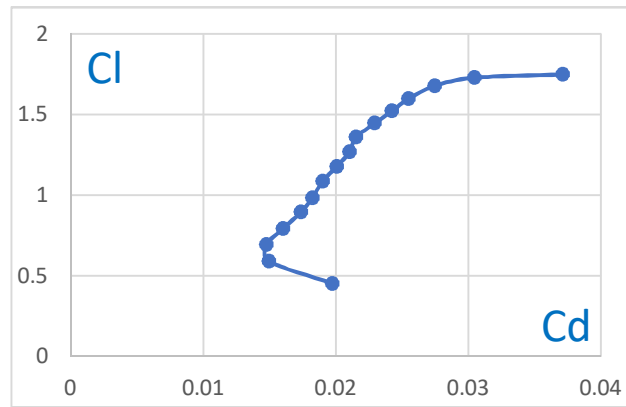
Figure 3.3 – *Lift characteristics and drag polar (Re = 200 000)*

Table 3.1 - *The aerodynamic characteristics of a clean S1210 airfoil (Re $= 200\ 000$)*

| $C_{D_{min}}$	$C_{L_{opt}}$	$C_{L_{max}}$	α_n	a_0	α_{kr}	$\left(\frac{x}{l}\right)_{ac}$	$\left(\frac{y}{l}\right)_{ac}$	$C_{m\ ac}$
0.012512	0.54	1.78	-9.79	0.0866	24.1	0.196063	-0.011458	-0.289736
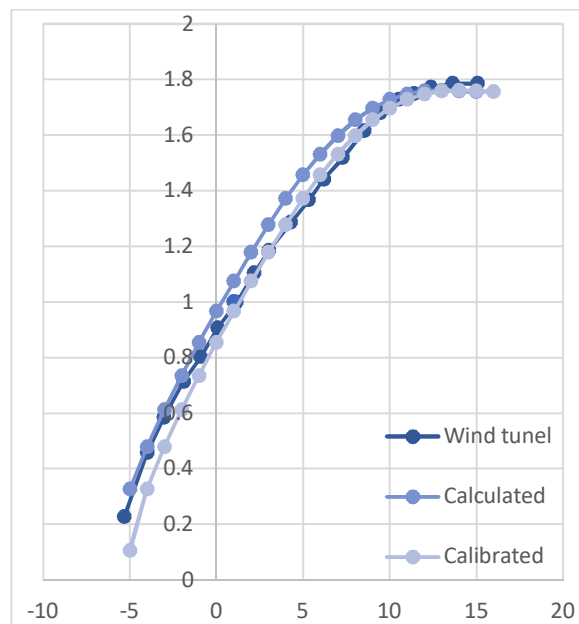
Figure 3.4 - *Calibrated airfoil lift curve (Re=200 000)*

The higher moment coefficient of the airfoil is the biggest flaw and it will be a challenge to set them in balance. The dimensioning of the horizontal stabilizer must include not only this fact but the possibility of moving the mass center towards the tail of the aircraft so that better maneuverability can be achieved. As the tail section carries more weight, their effective angles of attack are approaching positive values which will provide minimum drag of the horizontal stabilizer. As expected, values of angles of attack will still be negative and because of this, it is necessary to provide a minimal extension of the horizontal stabilizer.

This can be achieved with a smoothly curved airfoil on the stabilizer. The chosen airfoils are S 8025 and SD 8020 on the tail surfaces.

6

For the horizontal stabilizer, the chosen airfoil is the SD8020 because of its mild camber. Also, it is placed inverse because it is determined that the horizontal stabilizer will spend most of its time producing a negative lift. For the vertical stabilizer, the chosen airfoil is the S 8025.

3.3 WING DESIGN

As already mentioned, according to the rules of the competition, the dimensions of the aircraft are limited by the pre-flight box. This dependence directly affected both the dimensions of the wings and the dimensions of the horizontal tail. From figure 3.5 it can be seen that the aircraft will have the greatest wingspan when the tendon at the end of the wing touches the left, lower side of the rhomboid. Also, the wingspan will be larger for the larger wing narrow. Of course, the wingspan will be larger if the main diagonal of the pre-flight box is larger. If we observe isosceles triangle $A_0 B_0 C_0$ and express the height of that triangle (along $B_0 C_0$) over the angle of the pre-flight box and half of the wing chord at the end of the wing and subtracting half of the main diagonal of the rhombus, we get a half-span of the wing as a pre-flight box angle:

$$\frac{b}{2}(\alpha) = a \cdot \cos\left(\frac{\alpha}{2}\right) - \frac{n \cdot l_s}{2} \cdot \cot\left(\frac{\alpha}{2}\right)$$

From the previously obtained equation, it is clear that the wing will have the highest possible value for the smallest possible angles α, assuming that values of the root chord of the wing are fast as well as its narrow.
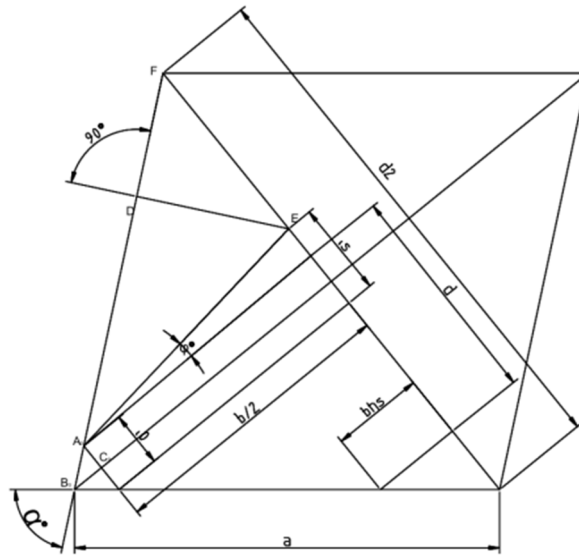

Figure 3.5 – Geometrical characteristics of the aircraft in the rhombus-shaped box

According to structural limitation, it is concluded that the maximum wingspan is $b = 2m$ and the maximum wing chord length is $l = 0.33m$. Also, the configuration of the wing that proved to be the most favorable is the trapezoidal shape of the wing in order to reduce the induced drag, the surface is S=0.2189, and the taper ratio is n = 0.5.
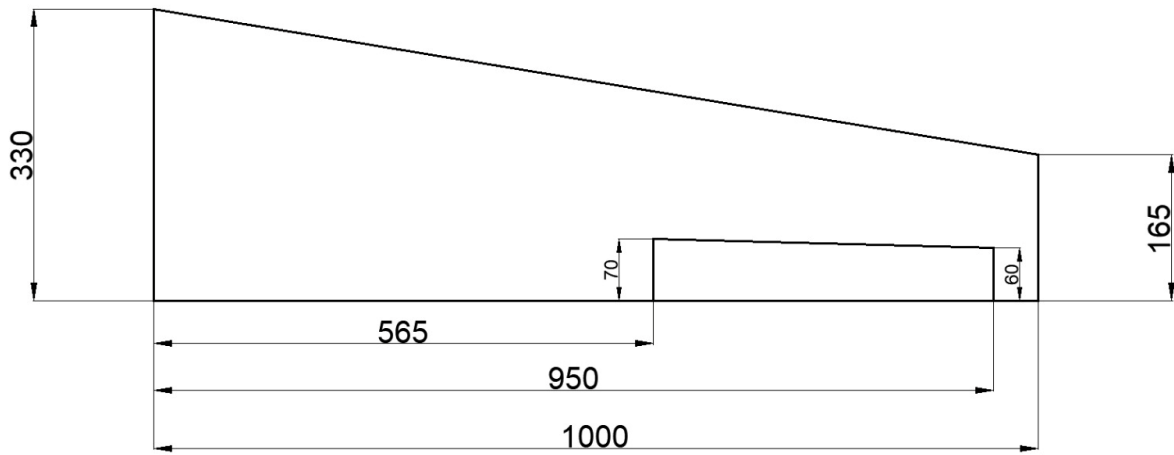
*Figure 3.6* - *The top view projection of the chosen wing geometry*
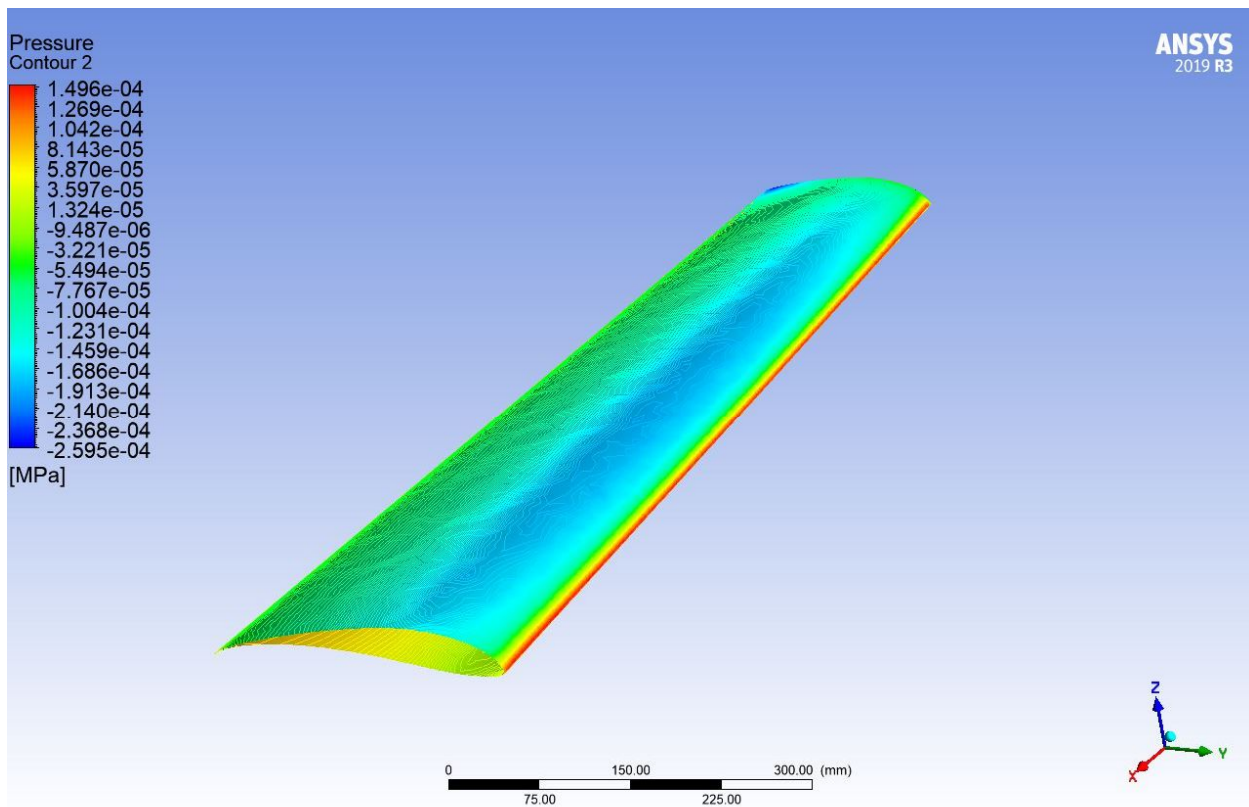
Figure 3.7 - *Pressure distribution along the half-wing*

3.4   HORIZONTAL STABILIZER

The airfoil creates high moment coefficients around the aerodynamic center, and so does the wing, so the contribution of the wings to the longitudinal static stability is a sizable one. Also, the large coefficients of lift and high drags contribute greatly, all this, and the influence of the fuselage

processed in section 4.2 must be countered with a horizontal stabilizer. This means that the horizontal stabilizer must be as efficient as possible (larger aspect ratio). The problems that arise with an aircraft this type (highly cambered airfoil on the wing) are difficulties to secure good maneuverability, enough stability, and small angles of attack of the horizontal stabilizer relative to the fuselage reference line. It is also important that the difference between the angles of the wing and the horizontal stabilizer is minimal. After numerous iterations, the horizontal stabilizer's final geometry and position were defined. Furthermore, the referent position of the aircraft's center of mass was chosen. Dimensions of the horizontal stabilizer are shown in the fig. 3.8.
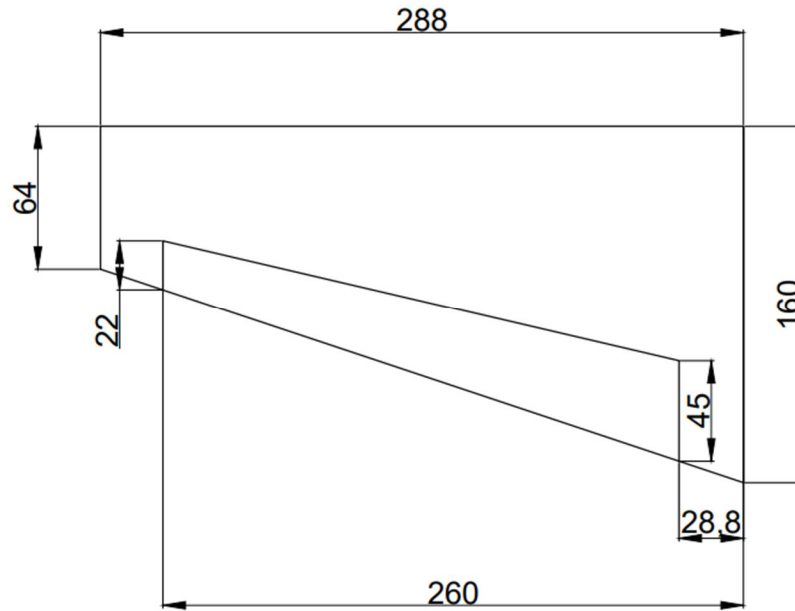

Figure 3.8 – Dimensions of the horizontal stabilizer

3.5   LONGITUDINAL STATIC STABILITY

The longitudinal static stability is influenced by all the elements of the aircraft that are exposed to the airflow, but also the position of the center of mass. When the wing and horizontal stabilizer are dimensioned, other existing elements need to be introduced and the diagrams of the moment change with the angle of attack and the lift coefficient has to be plotted. In this case, there is a relatively simple case where the contributions of the fuselage are negligible, as well as the contribution of the propulsion force (we will talk about these elements later). The aerodynamic surfaces of the wing and the horizontal fuselage have been replaced by their characteristic geometric quantities - the middle aerodynamic tendons (l_{sat}). The following assumptions are adopted: the aerodynamic center is located on the middle aerodynamic string and that the moment around the aerodynamic center is independent of the angle of attack that is valid in the linear domain.

The aerodynamic forces of drag, lift and the moment around the aerodynamic center of the wing. In the linear domain, as an approximation, it can be accepted that lift and drag have a grip in the aerodynamic center and that there will be a moment around the aerodynamic center independently of the angle of attack.
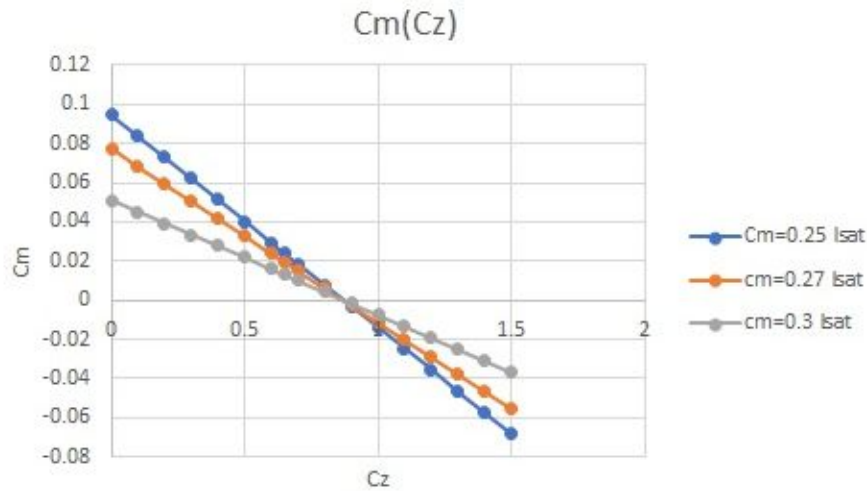
***Figure 3.9** - Longitudinal stability of aircraft according to the position of coefficient of the moment*

The impact of the fuselage and load carrier is the next important parameter that must be dealt with by using the semi-empirical method, as well as using Datcom. The analysis methodology with this program was reduced to the analysis of the contribution of the fuselage itself, by comparing it with the numerical method, and then adding other components of the aircraft and analysis with previously calculated values. As can be noticed, the gradient of the function does not differ much, but the free term, the coefficient of moment at zero angle of attack differs significantly.
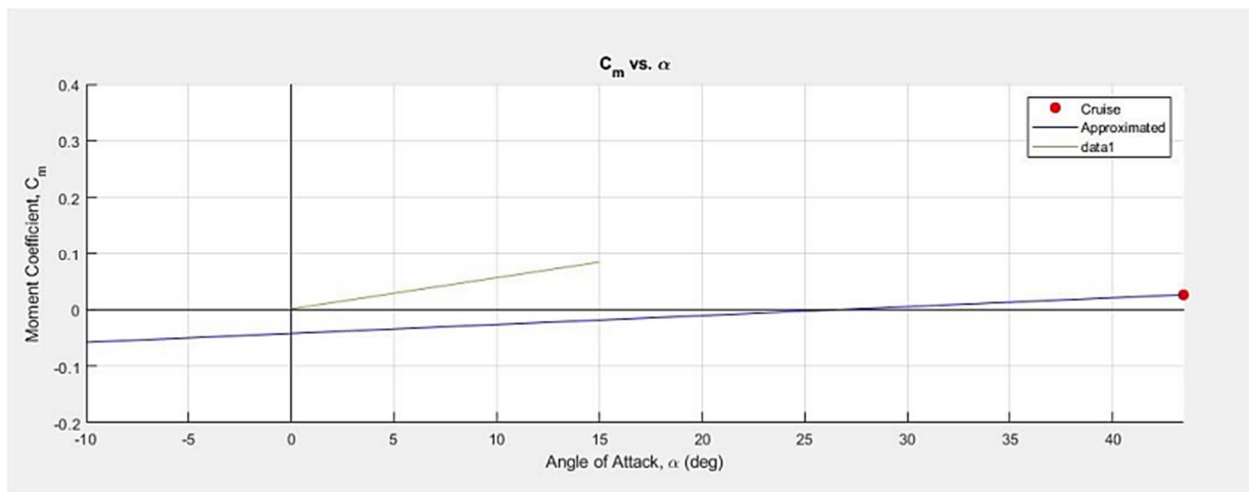

***Figure 3.10** – Contributions of the fuselage; Datcom (blue) and semi-empirical method (green)*

The next step is to analyze the entire aircraft. The figure above shows a comparison of the two methods. The values obtained by Datcom are marked in blue, while the values obtained analytically are marked in green. As can be seen in the diagram itself, the analytical method provides slightly more considerable stability than the numerical method, but both have the same intersection point. This tells us that our aircraft will be "trimmed" at approximately 2° of the angle of attack.
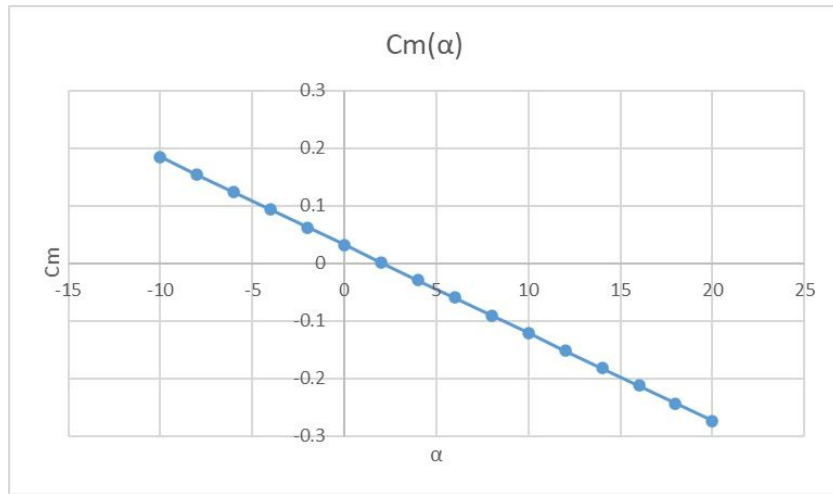
Figure 3.11 – Longitudinal stability of aircraft according to angle of attack (analytical)
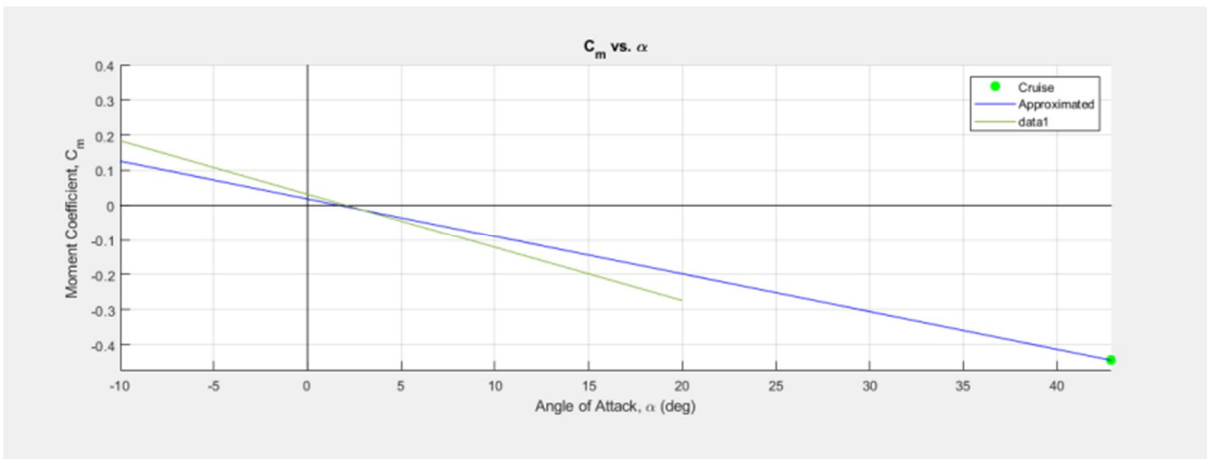

Figure 3.12 - Longitudinal stability of aircraft according to angle of attack; Datcom (blue) and semi-empirical method (green)

3.6 DIRECTIONAL AND LATERAL STATIC STABILITY

The contributions of the wings and fuselage are mostly destabilizing, however, in order for the aircraft to be stable in the direction, an aerodynamic surface is needed, which will have a dominant influence on the stabilizing contribution. This element represents the vertical tail, which in the full sense can be considered the basis of the directional stability of the aircraft. When the sliding angle appears, the angle of attack of the vertical tail also changes, the lift force is created on it and consequently the moment. If the vertical tail is placed behind the center of gravity of the aircraft, that moment will have a stabilizing effect. Dimensioning of the vertical stabilizer is one of the most important parts of the design. Bearing in mind that the efficiency of the vertical stabilizer is not the same in the presence of a horizontal stabilizer and without it, the dimensioning is based on the effective aspect ratio of the wing and the effective gradients of lift. The volumetric coefficient of the vertical stabilizer must ensure sufficient stability, but also sufficient space to have adequate steering in the presence of the rudder. The position of the center of mass also affects directional stability. After numerous iterations, the vertical stabilizer is designed.

Table 3.2 – *Contributions of each element individually*

Wing contribution	$(Cn\beta)_w$	0.00019
Fuselage contribution	$(Cn\beta)_f$	-0.0001
Influence of wing position	$\Delta_1\,Cn\beta$	0.0002
Vertical tail contribution	$(Cn\beta)_v$	0.00205
Influence of fuselage interferntion	$\Delta_2\,Cn\beta$	-0.0005

By summing the component, previously calculated values, stability in the direction is obtained: $Cn\beta$ = 0.002. Directional stability can be considered relatively small, but as the impact of the engine on this aircraft is relatively small, it is expected that this stability is sufficient for the aircraft to carry out its mission. Vertical stabilizer can be seen in figure 3.13.
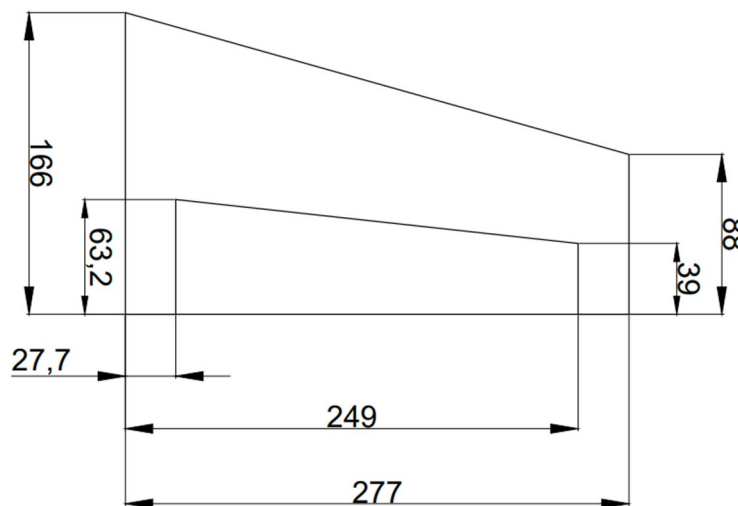
Figure 3.13 – *Vertical stabilizer*

3.7 AIRCRAFT PERFORMANCE

The performance of the plane is the end result of the project. Aircraft performance can be determined by analyzing the forces acting on an airplane in different positions. For the most part, performance can be determined by the required and available power.

Common methods for determining the performance of airplanes with reciprocating or turboprop engines are based on the ratio of required and available forces. Combining the aerodynamic characteristics of the clean configuration with the chosen power plant characteristics, the performance analysis could be calculated. Figures graphically show cruise, climb, glide and turn performances. Cruise speed is at 16m/s (57.6 km/h) and at Cz ≈ 0.9.
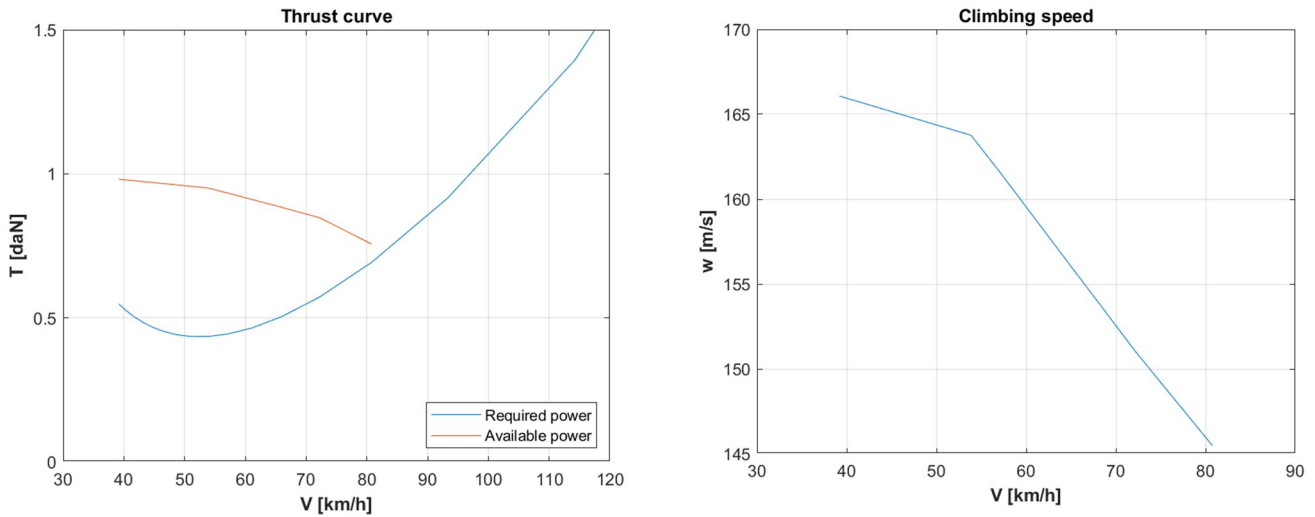
Figure 3.14 – Available and required thrust (left), Climbing speed (right)

3.8 PAYLOAD PREDICTION

Talking about this topic, mass of aircarft will be changed from its empthy weight $m_0 = 3.5$ kg to $m_1 = 7.1$ kg with step of 0.3 kg which is equal to mass of one bagg. Height will be calculated considering the performance given in figure 3.14 (rigth). Thus, density is simply given from the equation [4]:

$$\rho = \rho_0 \left(1 - \frac{h}{44300}\right)^{4.25588}$$

$$PREDICTED\ PAYLOAD\ [\text{kg}] = 165 \cdot \rho[\text{kg/m}^3] - 193.6$$
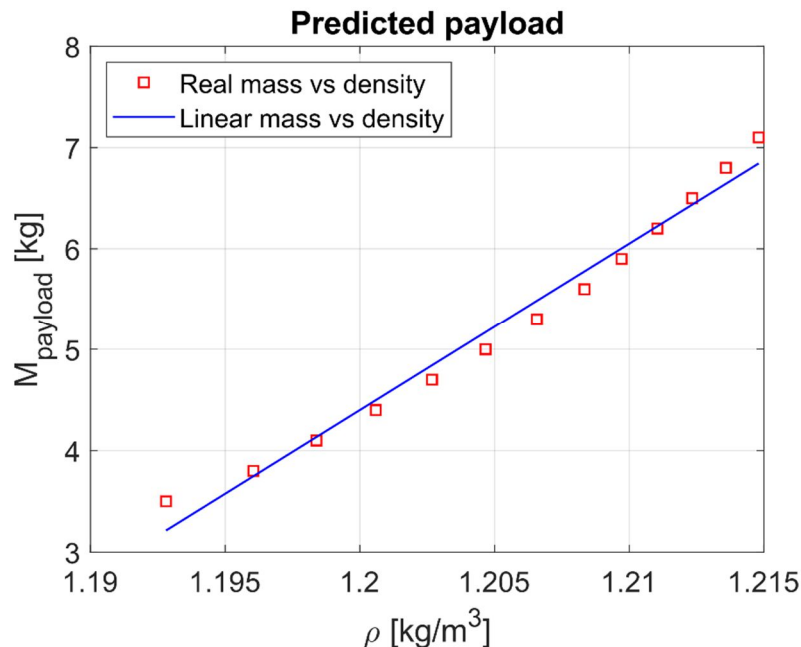
Figure 3.15 – Payload prediction

13

4 STRUCTURAL DESIGN

4.1 WING DESIGN

In order for a wing of such a high aspect ratio to carry an anticipated load, it is necessary to design a system of elements that transfer loads to one another. It consists of four spars, ribs and stringers. Carbon tubes were used for wing-fuselage connection. Also, connection is secured with a nut and bolt. The outer diameter of the carbon tubes in wings matches the inner diameter of tubes in the fuselage which ensures good fit and tolerance of the joint. These tubes are going through a series of ribs in the root section ensuring excellent load transfer from the wings to the rest of the aircraft.
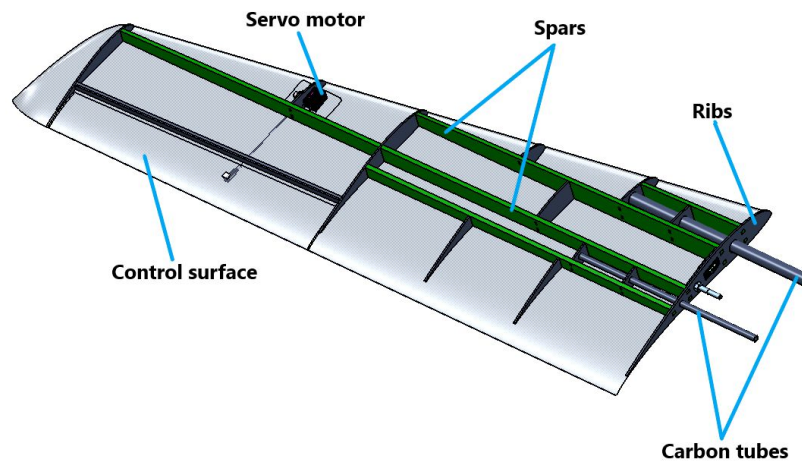

Figure 4.1 – Structure of the left wing

Most of the ribs are made of od airex-carbon sandwich. The skin of the wing is made of carbon fiber. Winglets are designed so that they can be manufactured as one part with the rest of the skin, thus avoiding any additional joints. The ailerons are positioned from 56.5% of relative half-span up to winglets. It has 30% of the local chord thus ensuring good maneuverability. Spars have openings of appropriate dimensions into which the pins on the ribs enter and thus their position is ensured.
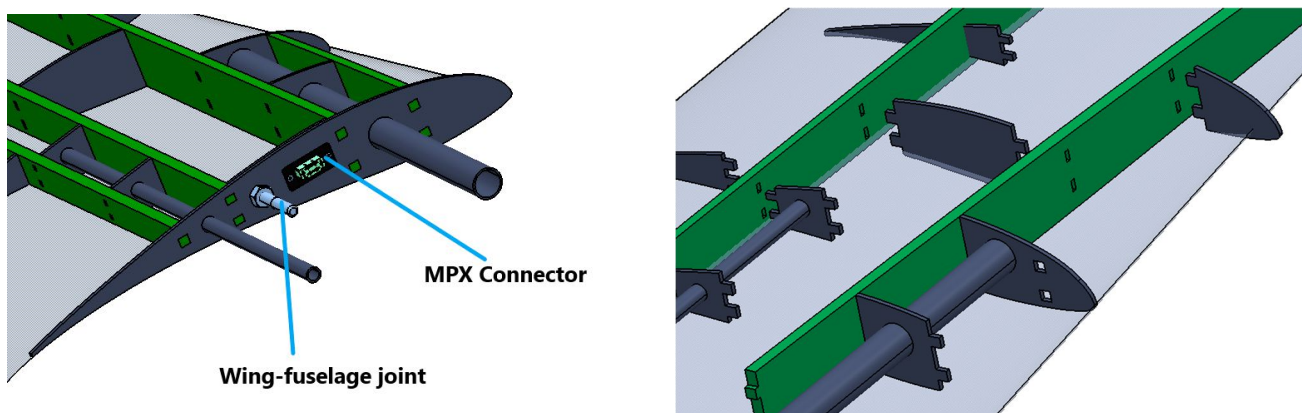

Figure 4.2 – Wing fuselage joint (left), Ribs-spars joint(right)

This method reduces the amount of glue needed to join the parts. The Servo motor is hidden inside the empty volume of the skin, but the linkage that connects the servo motor and control surface is located on the outside. One MPX Connectors was placed within the wing joint to ensure connection of servos placed in the wing with the rest of the electronics.
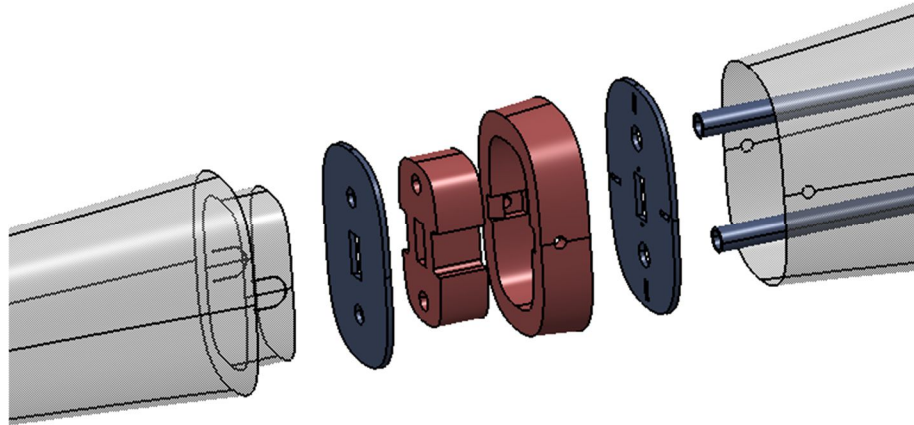

Figure 4.3 – Connection of the front and rear part of the fuselage

4.2   FUSELAGE DESIGN

The fuselage of the aircraft was designed to accommodate required payload, all structural elements needed and the necessary electronics and mechanical elements. The size and shape were optimized to ensure the minimal drag due to shape and skin friction. The aft part of the fuselage was designed in such a way to prevent the occurrence of the wake by ensuring a smooth transition from the fuselage to the tail section.
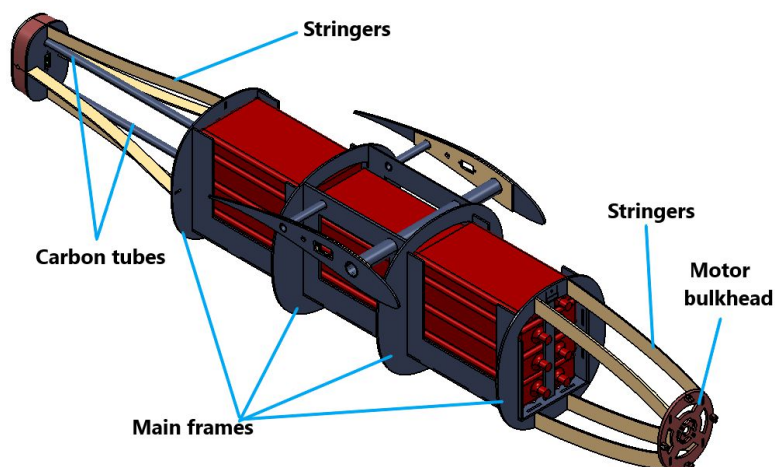

Figure 4.4 – Structure of fuselage

The fuselage is divided into two parts along the length so that it can fit in the transport box, and the overall dimensions are determined based on the limitations of the limiting box. The front is equipped

with cargo, electronics and batteries, while the rear is made with a vertical tail. The solution for the connection of the front and rear part of the fuselage is designed on the principle of male-female connection. In the front part of fuselage, at the joint, there is a two-part 3D plastic connector into which the rear part enters. The connection is strengthened by two carbon-airex frames on each side. Screws hold together this connection and skin of fuselage.

Main frames were made out of carbon–airex sandwich. They have multiple roles, one of which is to transfer loads from fuselage–wing joints to the skin of the body via ribs and spars. The rest of the structure is composed out of additional frames, skin, stringers made out of carbon – airex and fiberglass-airex sandwich and carbon tubes in the aft part of the fuselage to strengthen the weakest section. The skin is carbon laminate that changes thickness with respect to loads. The FEA structural analysis, was conducted to find the optimal laminate. Payload is located in the center of mass, so the changes of the mass and type of the payload wouldn't influence aircraft stability and possibly maneuverability. It sits on a perforated plate that separates cargo area and electronics bay. To ensure that the payload is fixed during the flight special measures were undertaken. The cargo of blood bags is located in the cargo bay and is stored in three compartments. Each section is surrounded by two frames. There is one vertical plate in each of the front and rear frames, which prevents axial movement of the payload, and the transverse movement is prevented by the frames themselves. The lid rests on a wreath and is locked with a pin mechanism.

4.3   CARGO BAY

The idea when designing the cargo space was to insert blood transfusion bags as easily and quickly as possible. It consists of retaining walls and base plate. It is divided into three partitions arranged along the longitudinal axis of the aircraft. In the front and rear compartments can be placed three bags of 300g and one of 200g, while in the middle can be placed three bags of 300g and one of 100g. The bags are stacked on top of each other through a lid located on the upper side of the fuselage. The total weight of the cargo is 3.2 kg.
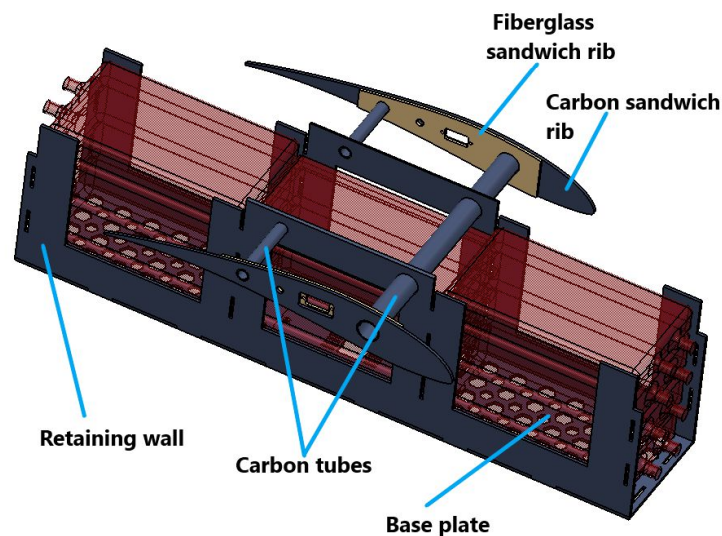

Figure 4.5 - Structure of the cargo bay

The Cargo Bay and fuselage combination is carried out without the aid of screws. Retaining walls and base are connected with the frames of the fuselage according to the puzzle principle and thus the movement of the cargo bay is prevented. The bags are compactly placed between the retaining walls so that their movement is prevented and the sloshing effect is reduced. Both the retaining walls and the base plate are made of sandwich construction - airex in the middle and one layer of carbon on each side. The base is perforated in order to reduce the total mass of the entire aircraft.

4.4   LANDING GEAR

At the beginning, it was necessary to decide on one of the two possible configurations for the landing gear. These are tricycle or taildragger configurations. Based on its characteristics, the taildragger configuration was chosen. It consists of a main landing gear and a tailwheel. Due to the differences in the height of the main landing gear and the tailwheel, the horizontal axis of the aircraft will not be parallel to the ground on which the aircraft stands. It was necessary to define all the geometric characteristics in order to avoid overturning the aircraft on the nose during landing.
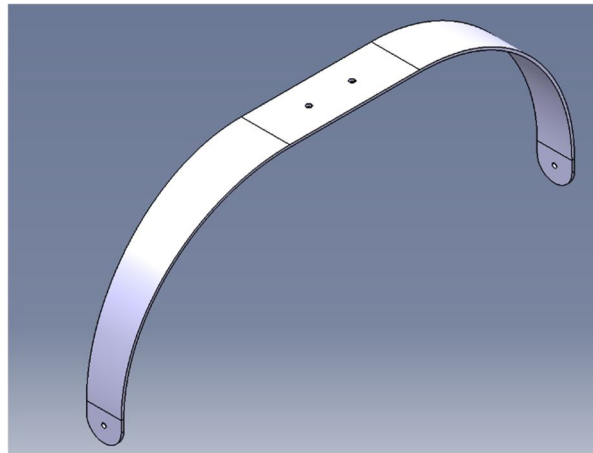

Figure 4.6 - *Main Landing gear*
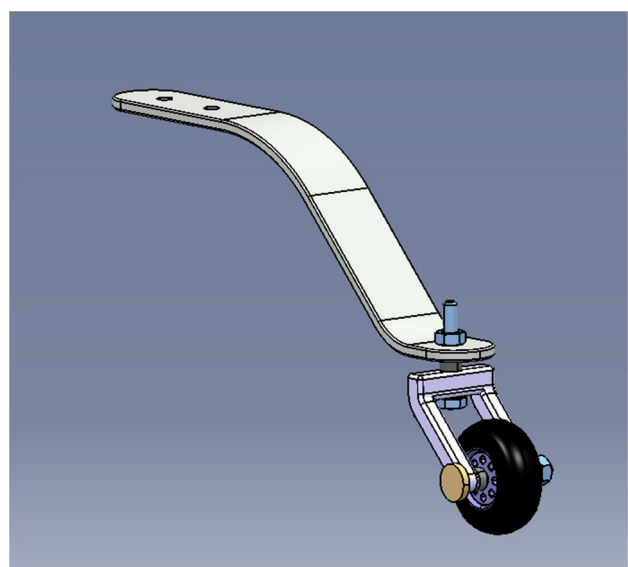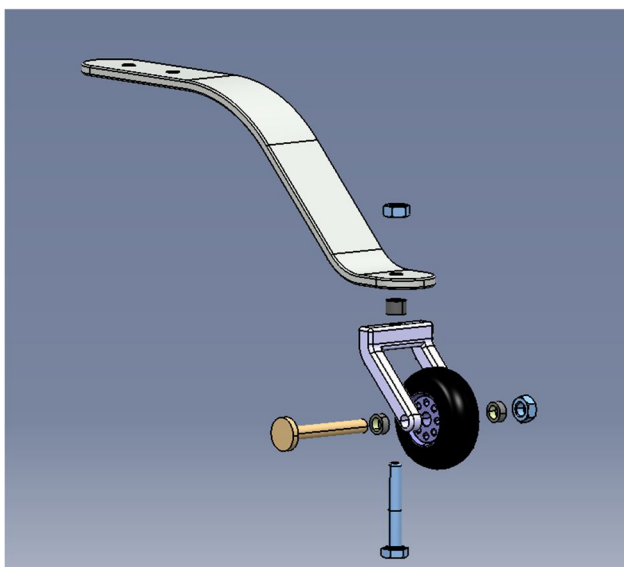
Figure 4.7 - *Parts of a tailwheel (left), Folded tailwheel (right)*

These geometric characteristics directly affect the dimensions and position of the landing gear in relation to the center of gravity. It was also necessary to optimize those dimensions and position so that the entire aircraft could fit in the limiting box. FEM analyses have included the static load of the aircraft and have calculated the load due to impulse of the force when landing in the domain of the vertical components of the speeds. The main landing gear and tailwheel are produced by the team. Main landing gear is made of carbon fiber and fiberglass, while tailwheel is made out of aluminum. The wheels are connected to the landing gear as illustrated on Figure 22.
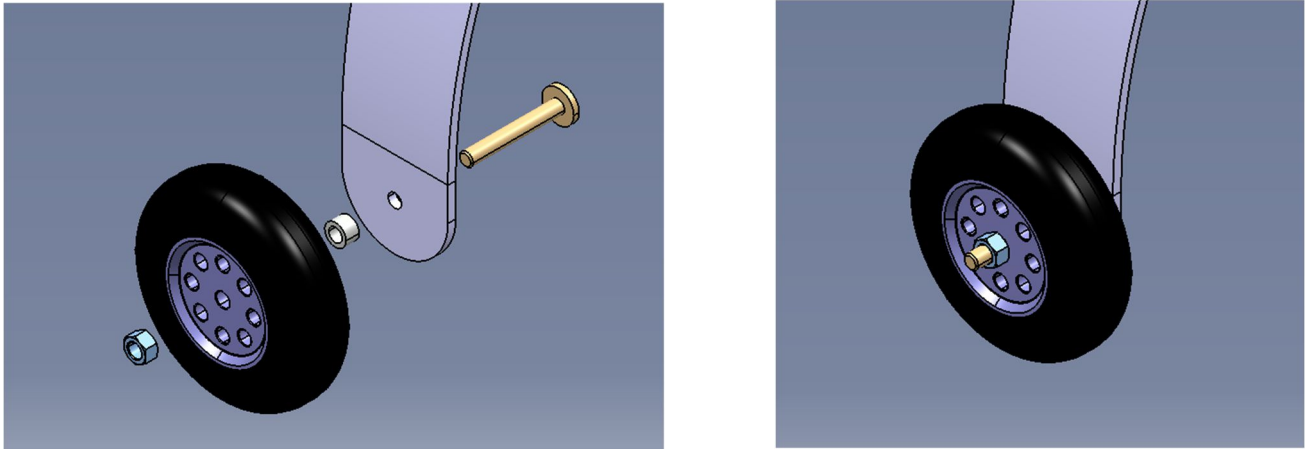
Figure 4.8 - Parts of a main landing gear (left), Folded main landing gear (right)

4.5 TAIL SECTION

The tail of the aircraft consists of a vertical and a horizontal stabilizer. The skin of the vertical tail is designed to be manufactured with the skin of the fuselage, so that ensures that no additional joints were needed. The structure of the vertical tail is composed of two spars, ribs and walls that enclose the control surface.
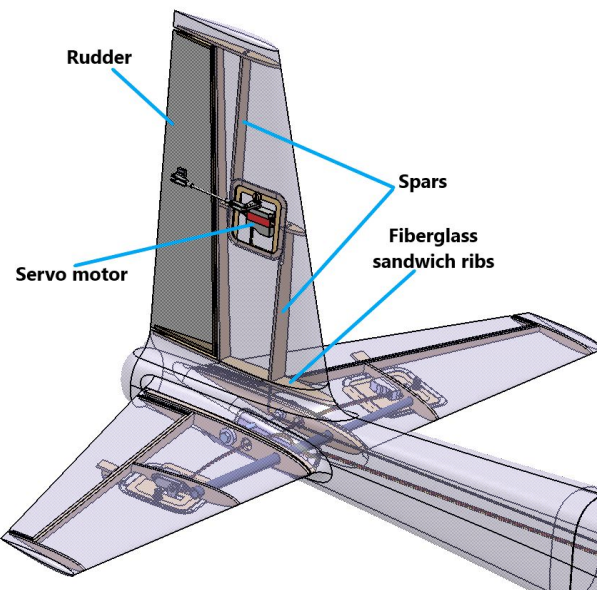
Figure 4.9 - Structure of the vertical tail

All of these parts are made of airex-fiberglass sandwich. Control surface is dimensioned in such a way that it has enough surface area so that the aircraft is easily controlled. Servo motor and linkage system is done similarly to the ailerons, meaning that it is hidden inside the empty volume of the skin.

Configuration of horizontal tail is conventional. The structure of the horizontal tail is made of carbon tubes, ribs and walls that enclose the control surface. Carbon tubes are spars. The tube in the left half-wing is of smaller diameter and enters a tube of a larger diameter that goes from the rib at the root to the right half-wing. The ribs at the joint of the carbon tubes are made of airex in the middle and one layer of fiberglass on each side. The reason of the greater thickness of these ribs is that there is a horizontal tail-fuselage connection. This connection consists of a bolt and nut and access to them is provided by a lid on the skin.

The servo motor mechanism is the same as in the vertical tail. Control surface at the horizontal tail ensures excellent maneuverability.
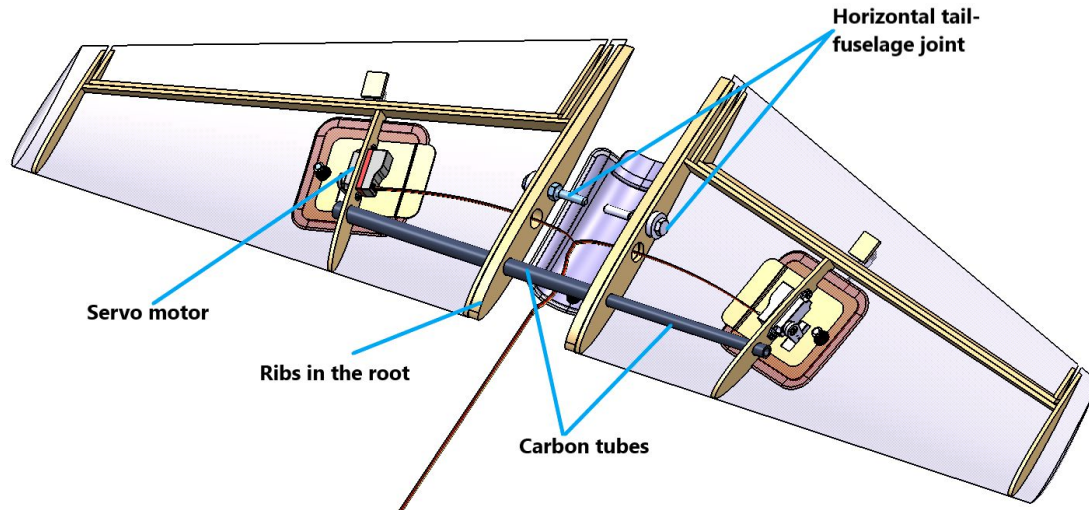
Figure 4.10 - Structure of the horizontal tail

5   PROPULSION

Propulsion system was tested in the wind tunnel for validation of the analytical results. For that purpose, velocity was varied from 0 to 25 m/s which is maximum velocity with step of 5 m/s. The goal was to get the propulsion force as a function of velocity, $T = f(V)$. All the results were obtained and noted in the Excel form in real-time using QuantumX and catmanEasy software. Duration of every test was approximately 20 seconds, with variation of power of 50, 75 and 100% for tested speeds.

We tested two propulsion systems – the first one with the Turnigy Nano-Tech 3000mAh 3S 30C battery, Aerostar RVS 40A BEC 3A ESC with reverse function and the APC 10x6E propeller, and the second system was with the Turnigy Nano-Tech 2650mAh 3S 30C battery, controller was Rics 30A and the Aeronaut CAMcarbon Light 10"x6" propeller. The same AXI 2826/10 GOLD LINE V2 motor

was utilized for both systems. It was observed that the first system produces higher overall thrust than the second one.

Aerodynamic and electronic characteristics were recorded and the following parameters are the
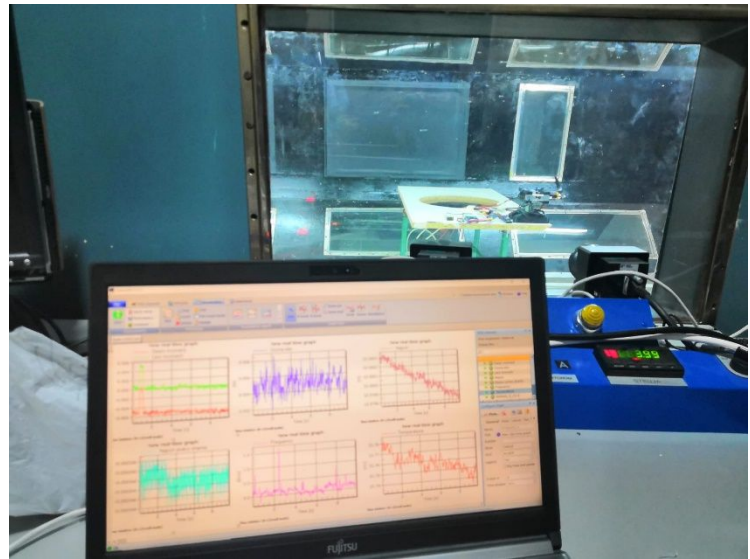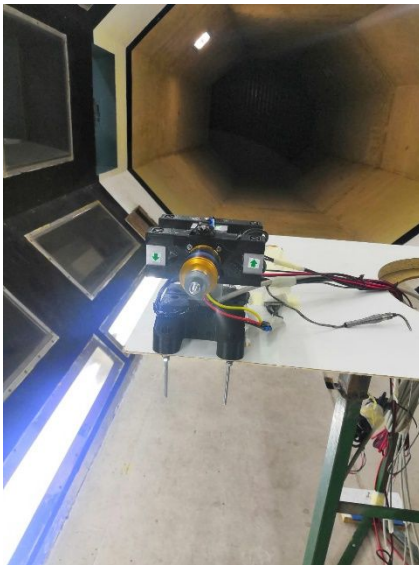
Figure 5.1 – Propulsion system in wind tunnel (left), Data stored in catmanEasy (right)

most important: thrust T [N]; power P [W]; motor rotation rate N [RPM]; voltage U [V]; current I [A]; efficiency η [%]. Maximum efficiency at cruise speed is: $\eta = 88.5$ %, while maximum thrust is: $T = 14.2$ N.

The battery was fully charged before test started with voltage of 12.6 V, whereas at wind tunnel air speed of 15 m/s the voltage was 11.3 V. The motor is connected with screws to test table which produces drag. It is worth mentioning that this drag will be lower than drag that produces fuselage because its frontal area is bigger than area of the test bench.
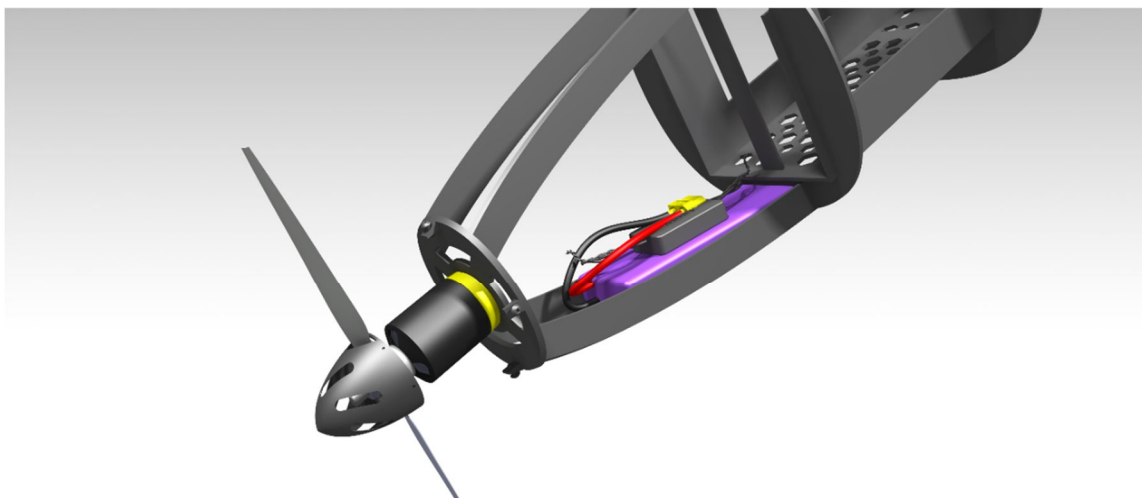
Figure 5.2 - Complete propulsion system placed in front part of the fuselage; motor is connected with screws to an engine mount; ESC is placed on the battery
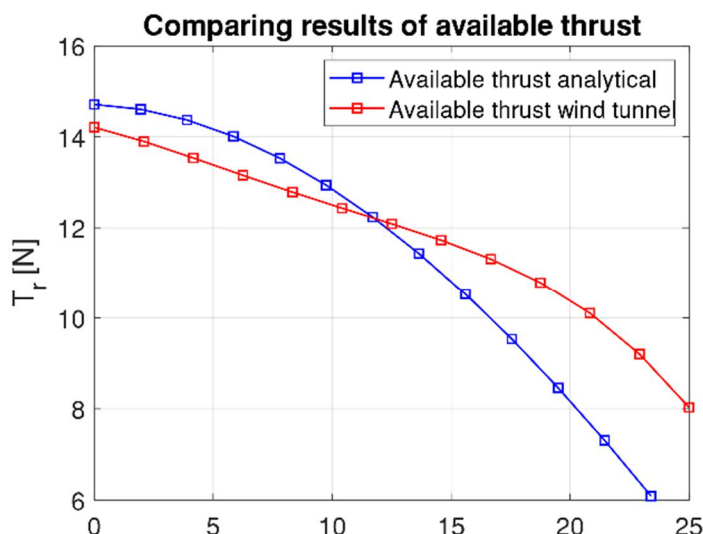
Figure 5.3 - *Available thrust measured in wind tunnel provide better results for higher air speed*

Table 5.1 – *Electric characteristics at air speed V = 15 m/s*

Throttle [%]	Current [A]	Voltage [V]	Rotation rate [RPM]	Power [W]	Efficiency [%]
50	9.2	12.04	11077	90.5	77.2
75	15.9	11.72	10745	166.3	84.5
100	27	11.31	10430	287	88.5

6 ELECTRONIC SYSTEM AND EQUIPMENT

In order for system to be completed, position, dimensions and power of servo motors must be determined, as for dimensioning and housing for cables. Housing of electronics itself doesn't affect aircraft center of mass. The ESC (Electronic Speed Controller), Aerostar RVS 40A BEC 3A ESC, is connected to main battery with gold plugs 3.5 mm and placed on top of battery. Two batteries are being used: Turnigy Nano-Tech 3S 30C 3000mAh for motor and Turnigy Nano-Tech 2S 1500mAh for receiver power source. Inside horizontal tail, two servo motors are located for aircraft control and they are connected to same PWM (Pulse Width Modulation) input pin on receiver module. On vertical tail there is another single servo motor connected to separate input pin on receiver. Those three servos ensure maneuverability over radio control. For automated measurements of flight, altitude and GPS data, we use Unilog GPS Logger 3 where the "LINK" cable with the three wires and the blue plug is plugged directly into a free servo port of receiver and supplies logger with power. Receiver module is FrSky_X8R with 16 channels, from which 8 are normal PWM outputs.

Figure 6.1 – Electronic components

7 MANUFACTURING

92% of the aircraft is made of composite materials with combination of carbon fibre sandwich sheets, sandwich core of Airex and 3D printed parts (PLA, SLA). It was decided that the process will be done with Vacuum resin infusion process. For the purpose of finding real properties of used materials, tensile and flexural testing was done. Results from these tests were used as a starting point for FEA analysis. The parts that must withstand huge loadings and for those that had to be really precise, were done from metal, mostly out of aluminum.

Figure 7.1 – Production of negative molds

For the purpose of creating carbon parts, it was decided to first make positive of the models, after which negative molds would be done in tooling gelcoat. This ensures best possible dimensional accuracy and enabled the team to prevent and perfect the model before the molds were created.

Positive models were made of MDF because it has good ratio of cost and material properties. This process was done on a CNC machine in our workshop. After processing on CNC machine, it was needed to prepare and paint mater models in such a way that it must be like glass finish. Optimization of rough stock had to be done so that the time on CNC machine is minimized. This means that we made wood laminates out of thinner MDF plates so it roughly represents desired shapes. With this method we have cut the time needed for CNC milling in half.

Figure 7.2 – Vacuum resin infusion process

After these negative molds were made, steel refoments were implemented to stiffen the molds. Carbon parts made from this mold were cut to its desired shape after which they were glued together with two component adhesive.

Ribs, stringers and other parts made from carbon-airex sandwich were made on waterjet and CNC machine, after which they were implemented in the structure of the aircraft.

8   OUTLOOK OF AIRCRAFT

Figure 8.1 – Front view of aircraft (Render)

Figure 8.2 – Back view of aircraft (Render)

9 ATTACHMENT

9.1   FEA ANALYSIS RESULTS
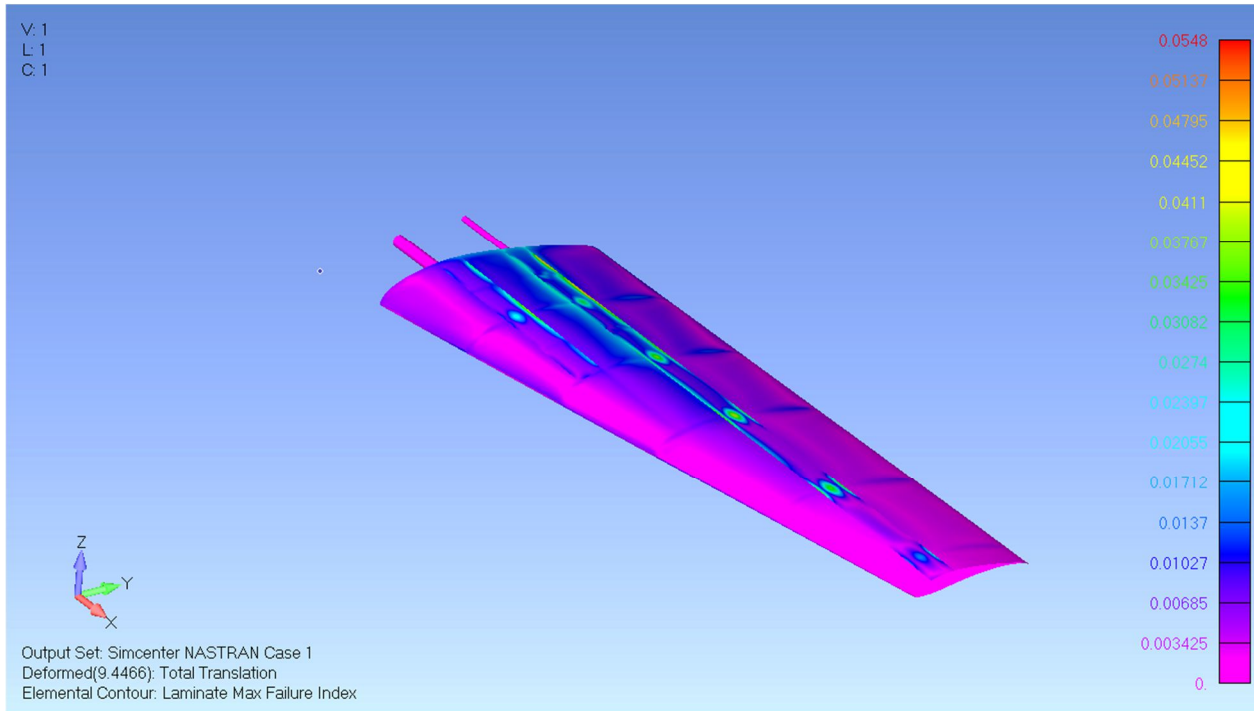
Figure 9.1- *FEA Wing*
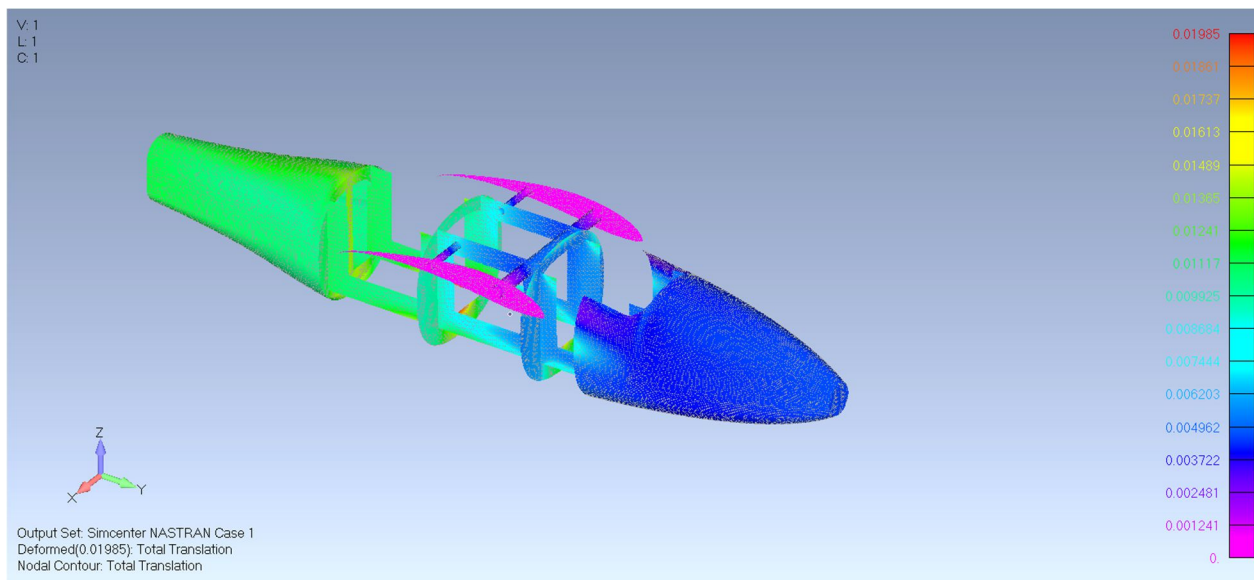
Figure 9.2 - FEA Fuselage
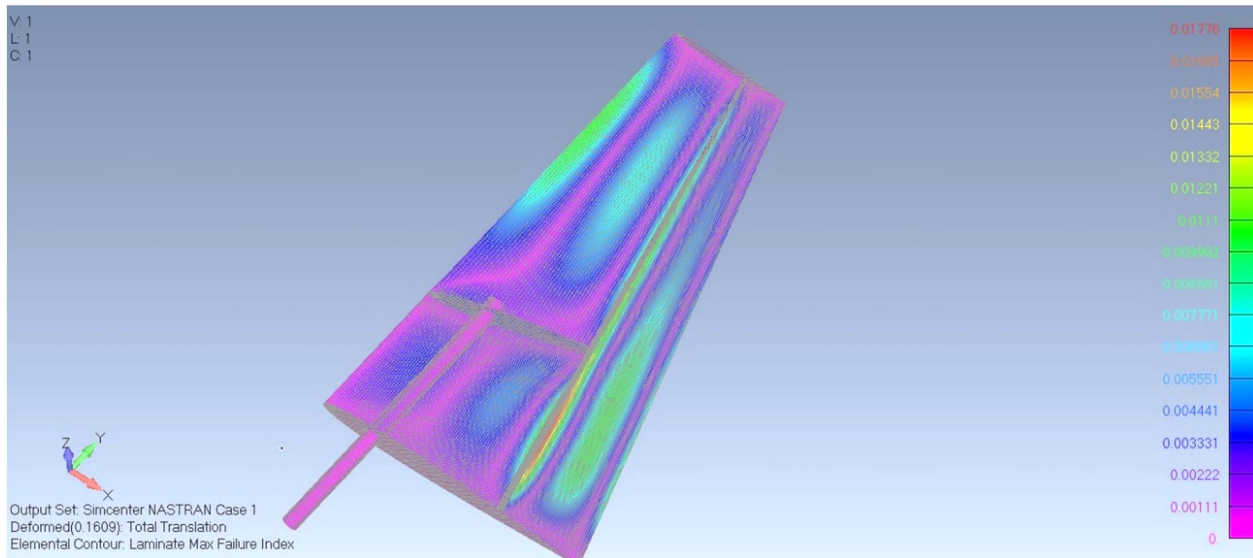
Figure 9.3 - *FEA Horizotal Tail*

9.2   MASS OF AIRCRAFT

Table 9.1 - *Mass of aircraft*

Mass of an aircraft		
Component name	**Mass (g)**	**Share [%]**
Wing (inner elements plus wing skin)	969.74	14.887
Fuselage (inner elements plus fuselage skin)	746.26	11.456
Horizontal tail (inner elements plus skin)	162.89	2.501
Vertical tail (inner elements plus skin)	79.56	1.221
Motor	205.00	3.147
Propeller	20.00	0.307
ESC	44.00	0.675
Main landing gear	245.00	3.761
Tail wheel	35.00	0.537
Battery 1	210.00	3.224
Battery 2	130.00	1.996
Payload	3200.00	49.126
Receiver	20.80	0.319
GPS (devices and box)	150.00	2.303
Cargo Bay	89.66	1.376
Motor Bulkhead	106.00	1.627
Wireing	100.00	1.535
Σ	**6513.906**	100

9.3 TECHNICAL DRAWINGS
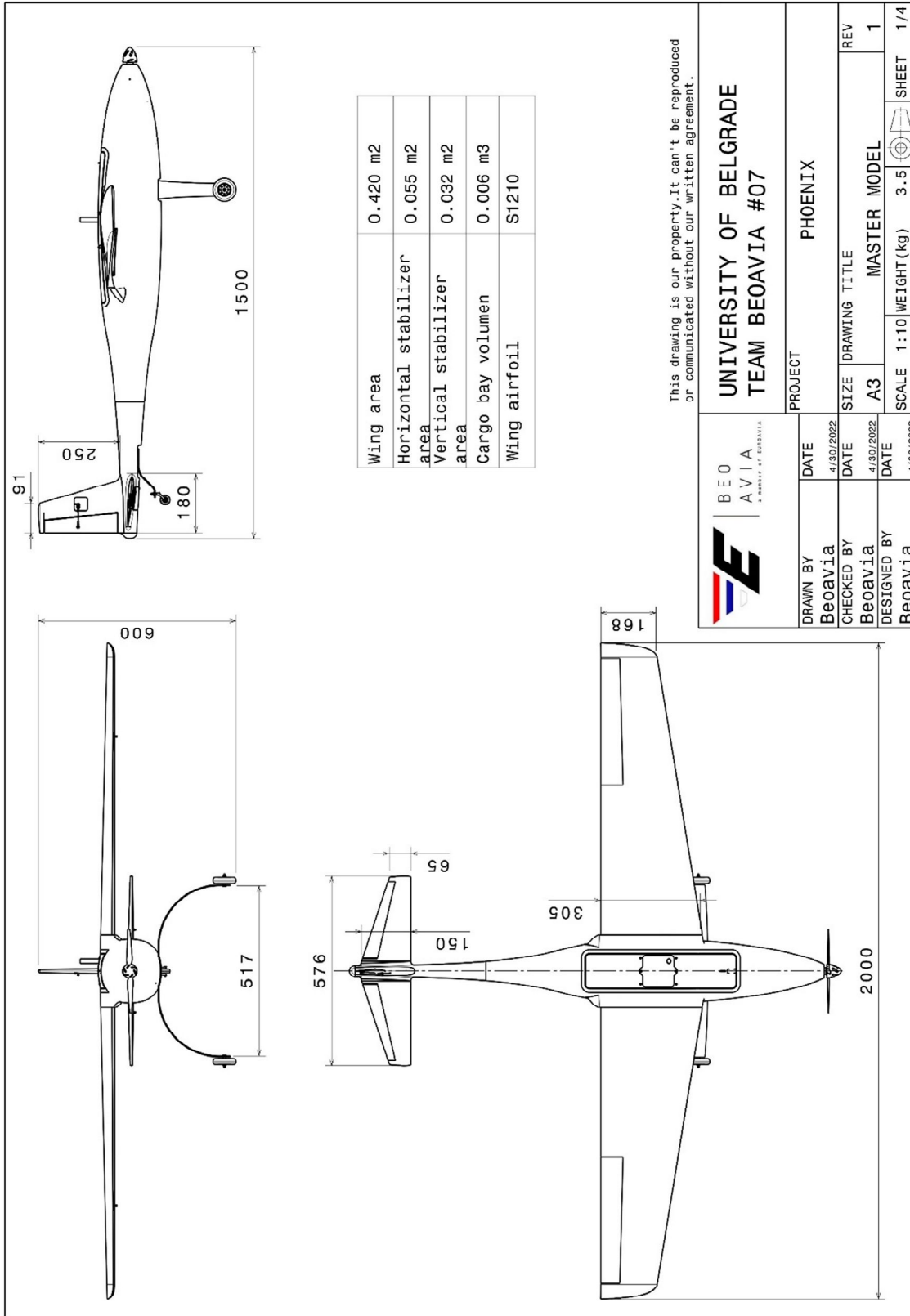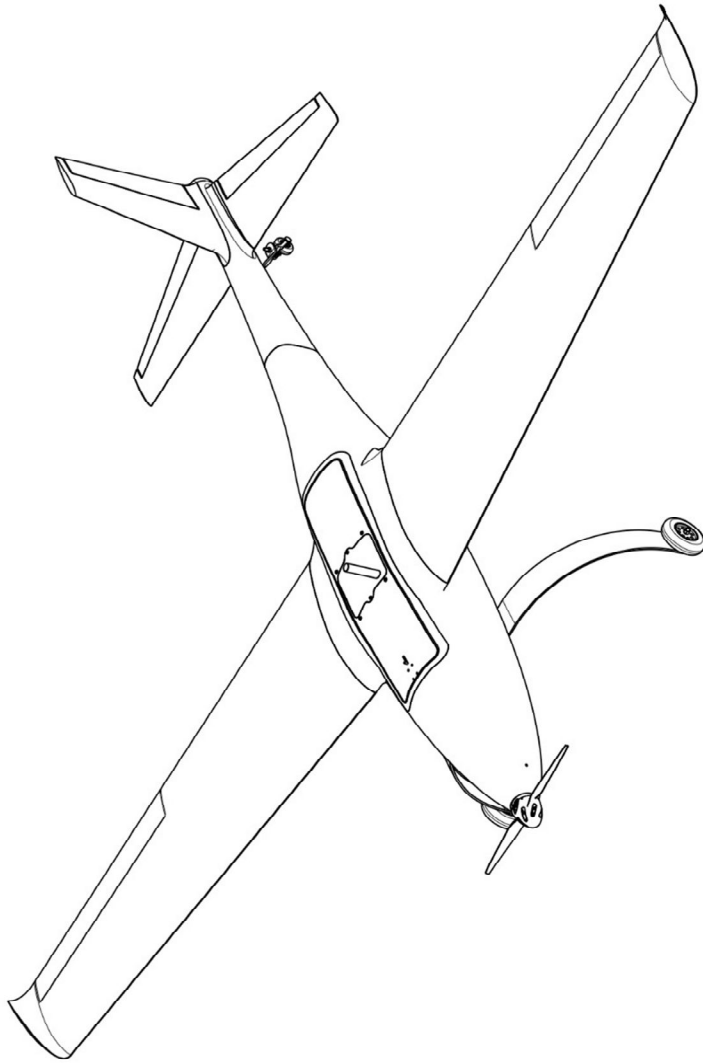
Wing area	0.420 m2
Horizontal stabilizer area	0.055 m2
Vertical stabilizer area	0.032 m2
Cargo bay volumen	0.006 m3
Wing airfoil	S1210

This drawing is our property.It can't be reproduced or communicated without our written agreement.

UNIVERSITY OF BELGRADE
TEAM BEOAVIA #07

PROJECT	PHOENIX			REV
SIZE	DRAWING TITLE			1
A3	MASTER MODEL			
SCALE 1:10	WEIGHT(kg)	3.5	SHEET	1/4

DRAWN BY	Beoavia	DATE	4/30/2022
CHECKED BY	Beoavia	DATE	4/30/2022
DESIGNED BY	Beoavia	DATE	4/30/2022

UNIVERSITY OF BELGRADE TEAM BEOAVIA #07				
PROJECT	PHOENIX			
SIZE	DRAWING TITLE			REV
A3	ISOMETRIC VIEW			1
SCALE	1:5	WEIGHT(kg)	3.5	SHEET 2/4

DRAWN BY	DATE	
Beoavia	4/30/2022	
CHECKED BY	DATE	
Beoavia	4/30/2022	
DESIGNED BY	DATE	
Beoavia	4/30/2022	

BEO AVIA

ITEM NO.	PART NUMBER	QTY.
1	Base plate	1
2	Retaining wall	2
3	Lid	1
4	RC reciver	1
5	Measuring equipment	1
6	Antenna	1

UNIVERSITY OF BELGRADE
TEAM BEOAVIA #07

BEO
AVIA
a member of EUROAVIA

This drawing is our property.It can't be reproduced or communicated without our written agrement.

DRAWN BY	DATE		PROJECT		PHOENIX			REV
Beoavia	4/30/2022							1
CHECKED BY	DATE		SIZE	DRAWING TITLE				
Beoavia	4/30/2022		A3	CARGO BAY				
DESIGNED BY	DATE		SCALE	1:5	WEIGHT(kg)	0.09	SHEET	3/4
Beoavia	4/30/2022							

This drawing is our property. It can't be reproduced or communicated without our written agreement.

UNIVERSITY OF BELGRADE
TEAM BEOAVIA #07

| PROJECT	PHOENIX			REV
				1
SIZE	DRAWING TITLE			
A3	COMPOSITE LANDING GEAR			
SCALE	1:2	WEIGHT(kg)	0.24	SHEET 4/4

DRAWN BY	DATE
Beoavia	4/30/2022
CHECKED BY	DATE
Beoavia	4/30/2022
DESIGNED BY	DATE
Beoavia	4/30/2022

BEO AVIA
a member of EUROAVIA

10 BIBLIOGRAPHY

[1] - "General aviation aircraft design: applied methods and procedures" – Gudmundsson Snorri; Embry-Riddle Aeronautical University 2014

[2] - "Applied aerodynamics - handouts" – prof. Ivan Kostić and prof. Olivera Kostić, University of Belgrade, Serbia, 2019

[3] - "Flight Mechanics" – Zlatko Rendulić, "Vojnoizdavački i novinarski centar", Belgrade, 1987.

[4] - "Aerodynamic constructions – handouts"– Ivan Kostić, Faculty of Mechanical Engineering, University of Belgrade, 2018

[5] - "Basics of Aerodynamic Constructions – Airfoils Part 1" –Miroslav Nenadović, University of Belgrade, "Prosveta", Belgrade

[6] - "Summary of Low-Speed Airfoil Data Volumes 1 - 5" – Michael S. Selig, James J. Guglielmo, Andy P. Broeren and Philippe Giguere, Christopher A. Lyon, Cameron P. Ninham, Ashok Gopalarathnam, Gregory A. Williamson, Bryan D. McGranahan, Benjamin A. Broughton, Robert W. Deters, John B. Brandt, Department of Aeronautical and Astronautical Engineering University of Illinois at Urbana-Champaign, SOARTECH PUBLICATIONS 1504 N. Horseshoe Circle Virginia Beach, USA 1995- 1997 and 201

[7] - "Airplane performance stability and control" – Courtland D. Perkins and Robert E. Hage

[8] - "Airplane Aerodynamics and Performance" – Dr. Jan Roskam, Dr. Chuan-Tau Edward Lan, Darcorporation, Lawrence Kansas, 1997

[9] - "Aircraft Stability and Control Part 1 and 2" - Miroslav Nenadović, University of Belgrade, "Zavod za grafičku tehniku Tehnološko-metalurškog fakulteta", Belgrade 1981 and 1984

[10] – "Methods for calculating aerodynamic characteristics" – Lazar Popović .